

**Proposal and analysis of a high-efficiency combined desalination and
refrigeration system based on the LiBr-H₂O absorption cycle
— Part 1: System configuration and mathematical model**

Yongqing Wang*

Cleaning Combustion and Energy Utilization Research Center of Fujian Province, Jimei University,
Xiamen, 361021, P. R. China

Noam Lior

Department of Mechanical Engineering and Applied Mechanics, University of Pennsylvania,
Philadelphia, PA 19104-6315, USA

Abstract: Simultaneous production of fresh water and refrigeration are often required, e.g. in warm-climate water-deficient regions, and this study is a proposal and analysis of an efficient way of producing both of them by consuming mainly low-grade heat. After introducing the configuration choice methodology, a combined refrigeration and water system, ARHP-MEE (Absorption Refrigeration Heat Pump and Multi-Effect Evaporation desalter), which is the integration of a LiBr-H₂O refrigeration unit, a LiBr-H₂O heat pump, and a low-temperature multi-effect evaporation desalination unit, is proposed, and the mathematical model is presented and validated. The model serves for conducting a performance analysis of the combined system, reported in Part 2 of this two-part paper.

Keywords: Integrated refrigeration and desalination system; Refrigeration; Water desalination; Combined cycles; Absorption refrigeration/heat pump; Multi-effect evaporation water desalination; Cogeneration

Nomenclature

C — Salinity of saline water [ppm] [g/kg]
 c_p — Specific heat capacity at constant pressure [kJ/kg K]

* Corresponding author. Tel.: +86-592-6180597; fax: +86-592-6183523.

E-mail address: yongqing@jmu.edu.cn (Yongqing Wang)

COP	—	Coefficient of performance
e	—	Specific exergy [kJ/kg]
E	—	Exergy [kW]
E_n	—	Energy [kW]
h	—	Specific enthalpy [kJ/kg]
H	—	Enthalpy [kW]
L	—	Latent heat of vaporization [kJ/kg]
m	—	Mass flow rate [kg/s]
p	—	Pressure [kPa] [MPa]
PR	—	Performance ratio
Q	—	Thermal energy; heat load [kW]
r	—	Relative error
R	—	Gas constant [kJ/kg K]
RWR	—	Refrigeration-water ratio [kJ/kg]
s	—	Specific entropy [kJ/kg K]
S	—	Entropy [kW/K]
T	—	Temperature [°C] [K]
v	—	Specific volume [m ³ /kg]
W	—	Work [kW]
X	—	Mass concentration of LiBr-H ₂ O solution [%]
Y	—	Mass fraction
Z	—	Molar fraction
ε	—	Exergy efficiency [%]
η	—	Adiabatic efficiency [%]
ξ	—	Non-dimensional exergy destruction [%]

Abbreviations and subscripts

A	—	Absorber
AHP	—	Absorption heat pump
AR	—	Absorption refrigeration
ARHP	—	Absorption refrigeration heat pump

b	—	Brine
c	—	Condensate
CD	—	Condenser for desalination
ch	—	Chemical
d	—	Destruction
ED	—	Evaporator for desalination
ER	—	Evaporator for refrigeration
f	—	Feed seawater; formation
F	—	Flashing box
g	—	Generation
G	—	Generator
H	—	Seawater preheater
in	—	Input
max	—	Maximum
out	—	Output
P	—	Pump
ph	—	Physical
R	—	Refrigeration
s	—	Salt
SC	—	Subcooler
SH	—	Solution heat exchanger
sw	—	Seawater
T	—	Thermal
TVC	—	Thermal vapor compression
v	—	Vapor
V	—	Throttling valve
w	—	Water
0	—	Dead state for exergy analysis; ambient
1, 2, ...	—	States on the system flow sheet

Superscripts

1. Introduction

Polygeneration systems, i.e. those that simultaneously generate more than a single product, are often more energy-efficient than those making the same products by separate single-product systems, with the significant advantages having been verified by both theoretical analyses and practical running results from an increasing number of installed poly-generation plants, of which power/heat cogeneration, power/water cogeneration and power/heat/refrigeration tri-generation are the most representative [1-3]. Well-understood from thermodynamic Second-Law considerations, the synergy is created mainly by proper driving force and exergy cascading of streams within the system.

A typical situation exists, e.g. in warm-climate water-deficient regions, where the simultaneous production of fresh water and refrigeration are required, and here we propose and analyze a polygeneration system that would produce both at a higher energy efficiency than two separate systems, one being a water desalination system that produces fresh water only and the other a refrigeration system that produces cooling only.

Only few past studies have addressed the concept of refrigeration and desalination cogeneration systems [4-8]. Aly [4] proposed a system composed of a LiBr-H₂O absorption machine and a 20-effect multi-effect evaporation (MEE) water desalination unit where the MEE replaces the condenser and evaporator of the single-purpose absorption refrigeration machine. It was predicted to have an evaporation temperature range of 6-63 °C, and to produce fresh water at a performance ratio (mass ratio of produced fresh water to consumed motive steam) of 14.2, plus a by-product of cooling capacity derived from the last-effect rejected brine with temperature of 6.8 °C. A recent paper by Gude and Nirmalakhandan [5] proposed a somewhat similar system where the heat for a single-effect distillation unit was that rejected from an absorption refrigeration condenser at a desalination efficiency of up to 90%, and producing refrigeration at the same time, but an overall energy or commercial feasibility index was not offered. Hou et al [6] proposed a system integrating an air-vapor compression refrigeration system, a humid-air dehumidification process, and a flash desalination process. Shen et al [7] and Hu et al [8] discussed the feasibility of providing the heat for a desalination process from an air-conditioning unit

exhaust heat, to produce cold energy alongside with fresh water. In present study, we proposed a combined desalination and refrigeration system with good thermodynamic performance and potential economic benefits. Different from the mechanically-driven systems in [6], the proposed system consumes mainly low-grade heat as those discussed in [4], [5], [7] and [8], and is suitable to be combined with the industrial processes that can provide that kind of heat, to improve the total energy efficiency. Although integrated also by an absorption unit and a MEE, the proposed system differs from that discussed in [4] by applying a conventional MEE unit with evaporation temperatures of 40-70 °C instead of an unconventional MEE containing nine evaporators working at 6-30 °C [4]. Owing to the high vacuum and low heat transfer coefficients caused by the low evaporation temperatures, the value of the MEE proposed in [4] remains doubtful. Different from the system described in [5] that focused on a one-effect evaporation desalination process coupled with an absorption air conditioning process, and from the systems in [7] and [8] that provided only general ideas of running desalination processes with air conditioner exhaust heat, our study illustrates the system integration logic and presents detailed thermal performance predictions including a parametric sensitivity analysis, a rough economic evaluation, and thorough discussions, of the proposed system.

The proposed system is based on the synergetic opportunity that absorption refrigeration (AR), absorption heat pump (AHP) and thermal desalination systems are all run by thermal energy with overlapping operating temperature regions, as shown in Fig. 1. Driven by low grade heat, say, 0.13-0.9MPa steam [9], a LiBr-H₂O AR unit produces refrigeration by evaporating refrigerant water at around 5 °C, and releases waste heat to the ambient. Also driven by such low-grade heat, a LiBr-H₂O AHP absorbs heat from the ambient (air or water), and produce heat with temperatures above ambient and below that of the driving heat source. At the same time, the top brine temperature of MEE typical water desalination systems is limited to a maximum of 70 °C to reduce scaling and corrosion [10], and its driving steam top condensation temperature is thus about 72 °C, just within the temperature range of the AHP output. Examining AR and AHP, we note that (1) an AR outputs refrigeration, as well as heat at a temperature close to the ambient (to maintain a high efficiency of refrigeration production [9]) and thus too low to run an MEE; (2) an AHP can supply heat with the temperature high enough to run MEE, but produces no refrigeration; (3) the proposed combination of AR and AHP, called ARHP (Absorption Refrigeration Heat Pump), can produce both refrigeration and desalination heat, and good synergy is expected because that AR and AHP work on the same thermodynamic principles (both work on reversed cycle and transfer heat

from a low-temperature medium to a high-temperature one), have similar configurations (both are composed of generator, absorber, evaporator, condenser, etc.), use the same working fluids (LiBr-H₂O solution and water/steam), and operate in overlapping temperature regions (as mentioned above and shown in Fig. 1), providing great opportunities and convenience of cascade utilization of energy/exergy streams within the system.

Fig. 1 Schematics of AR, AHP and ARHP

Following this logic, a combined refrigeration and water system integrated by AR, AHP and MEE and driven by low-grade heat, was configured and modeled in this paper, which is Part 1 of a two-part paper. Part 2 (a separate paper), contains the thermal performance analysis including a parametric sensitivity analysis, a rough economic evaluation, and their conclusions.

2. System configuration

The proposed combined desalination and refrigeration system, ARHP-MEE system, is composed of two subsystems: a single-effect LiBr-H₂O ARHP and an MEE desalter, with the configuration schematically shown in Fig. 2. The driving steam (1) heats the LiBr-H₂O mixture in the generator G and boils off the water in it. This steam (9) generated in G is routed into the evaporator, ED₁, of the first effect of MEE, providing the heat for seawater evaporation by releasing its sensible and latent heat. Its condensate (10) is subcooled by the ambient seawater, throttled and then introduced into the ARHP evaporator ER to produce refrigeration. The refrigerant vapor (13) from ER enters the absorber A, and the absorption heat is taken away by the cooling seawater (16). It is clear that the two subsystems are linked by ED₁, which is both the condenser of the ARHP and the evaporator of the MEE. Detailed description of the working process of MEE can be found in [11].

Fig. 2 Schematic diagram of the ARHP-MEE cogeneration system

In a typical refrigeration-only AR unit (Fig. 3), the condensation temperature (at 10) is usually around 40 °C, while in our proposed configuration it is raised to above 60 °C by regulating the operating parameters of the absorber A and the generator G, to produce the temperature required for MEE desalination. Producing refrigeration (in ER) and heat (in ED₁) simultaneously, the ARHP unit works as both a

refrigeration unit and a heat pump.

Fig. 3 Schematic diagram of the AR refrigeration-only system

In an AHP-driven MEE water-only system as shown in Fig. 4, part of the vapor (10) produced in the last effect of MEE is entrained by the absorber A and the absorption heat is used to heat and vaporize part of the condensate (11) from ED_1 . The vapor (9) formed in the generator together with that (12) from A serves as the heat source for the MEE. Compared with such an AHP-MEE, the production of refrigeration in the proposed ARHP-MEE is at the expense of the reduction of water production, because the absorber in the ARHP-MEE entrains the low-temperature/pressure vapor from the evaporator ER, causing the absorption heat temperature to become too low to produce vapor for driving the MEE. The result is that only the vapor (9) from the generator serves as the heat source for desalination and this reduces the water production rate. AHP-MEE systems have been studied by a few researchers [12-14], and the results indicate a competitive thermal performance (the economics were not addressed). For instance, Mandani et al. [13] performed a thermal analysis of a single-effect evaporation desalination process combined with a single-effect LiBr-H₂O AHP, and claimed performance ratios of 2.4-2.8, 50%-70% higher than the single-effect thermal vapor compression (TVC) systems driven by the same heat source. Su et al. [14] studied a water-production-only system composed of a double-effect LiBr-H₂O AHP and a 9-effect MEE, obtaining a performance ratio of 17.15, much higher than the 11.05 of a TVC-MEE system.

Fig. 4 Schematic diagram of the AHP-MEE water-only system

Our study presented in Part 2 of the paper shows that, when both refrigeration and fresh water are needed and low-grade heat is available, ARHP-MEE can obtain high energy saving, compared with the refrigeration-only AR unit and water-only AHP-MEE unit.

3. Mathematical modeling

It is assumed that the system operates in steady state, the heat losses through the system components are negligible, the refrigerant in ARHP is pure water and the produced water by MEE is salt-free. The principles of mass and species conservation, and First and Second Laws of thermodynamics are employed to build the mathematical model of the two subsystems, ARHP and MEE, of the combined system, and

the performance criteria are defined, and the modeling is validated.

3.1 Mathematical model for the ARHP subsystem

Following the mass conservation principle, the governing equations of mass balance, involving the mass balance of each species of the solution, for each component can be obtained, with the two main equations for ARHP shown below:

$$m_5 X_5 = m_6 X_6 \quad (1)$$

$$m_5 = m_6 + m_9 \quad (2)$$

Energy balances and heat loads for the ARHP components are:

$$Q_G = m_1(h_1 - h_2) = m_6 h_6 + m_9 h_9 - m_5 h_5 = Q_{in} \quad (3)$$

$$Q_A = m_8 h_8 + m_{13} h_{13} - m_3 h_3 = m_{15}(h_{16} - h_{15}) \quad (4)$$

$$Q_{SH} = m_6(h_6 - h_7) = m_4(h_5 - h_4) \quad (5)$$

$$Q_{SC} = m_{10}(h_{10} - h_{11}) = m_{14}(h_{15} - h_{14}) \quad (6)$$

where Q_{in} is the thermal energy input to the ARHP subsystem, which is also the thermal energy input to the whole ARHP-MEE system. The ARHP subsystem has two useful outputs: thermal energy Q_T by condensing steam (stream 9 in Fig.2) in ED₁ and refrigeration Q_R by evaporating the refrigerant (stream 12 in Fig. 2) in the evaporator ER,

$$Q_T = m_9(h_9 - h_{10}) \quad (7)$$

$$Q_R = m_{13}(h_{13} - h_{12}) \quad (8)$$

The energy balance for the whole ARHP subsystem is:

$$Q_G + Q_R + W_{P1} = Q_A + Q_{SC} + Q_T \quad (9)$$

where W_{P1} is the work consumption of the weak-solution pump P1,

$$W_{P1} = m_3(h_4 - h_3) \approx m_3 v_3 (p_4 - p_3) / \eta_{P1} \quad (10)$$

According to the second law of thermodynamics [15], exergy destruction, E_d , attributed to process irreversibility can be calculated by

$$E_d = T_0 S_g \quad (11)$$

where T_0 is the dead-state (here ambient) temperature, and S_g is the entropy generated due to process irreversibility, which can be calculated using the entropy balance equation for steady-flow process:

$$\sum m_{in} s_{in} + \sum \frac{Q}{T} + S_g = \sum m_{out} s_{out} \quad (12)$$

where s_{in} and s_{out} are the specific entropy and m_{in} and m_{out} the mass flow rate, of the working fluids entering and leaving the analyzed control volume, respectively, Q is the heat rate transferred through the system boundary at temperature T and the summation is over all respective mass flows and heat inputs and outputs, into and from the analyzed control volume. Applying Eqs. (11) and (12), the exergy destruction in each component of ARHP can be written as

$$E_{d,G} = T_0 (m_2 s_2 + m_9 s_9 + m_6 s_6 - m_1 s_1 - m_5 s_5) \quad (13)$$

$$E_{d,A} = T_0 (m_3 s_3 + m_{16} s_{16} - m_8 s_8 - m_{13} s_{13} - m_{15} s_{15}) \quad (14)$$

$$E_{d,SH} = T_0 (m_7 s_7 + m_5 s_5 - m_6 s_6 - m_4 s_4) \quad (15)$$

$$E_{d,SC} = T_0 (m_{11} s_{11} + m_{15} s_{15} - m_{10} s_{10} - m_{14} s_{14}) \quad (16)$$

$$E_{d,V1} = T_0 (m_8 s_8 - m_7 s_7) \quad (17)$$

$$E_{d,V2} = T_0 (m_{12} s_{12} - m_{11} s_{11}) \quad (18)$$

$$E_{d,P1} = T_0 (m_4 s_4 - m_3 s_3) \quad (19)$$

$$E_{d,P2} = T_0 m_{14} (s_{14} - s_{sw,0}) \quad (20)$$

The cooling seawater (stream 16 in Fig. 2) at a temperature higher than the ambient has potential to do work, that is, contains exergy. Usually, this exergy is not used but destroyed in the process where the cooling seawater changes its temperature and pressure to that of the ambient, thus causing exergy destruction:

$$E_{d,16} = m_{16} [(h_{16} - h_{sw,0}) - T_0 (s_{16} - s_{sw,0})] \quad (21)$$

Thermal exergy and cold exergy output by ARHP are:

$$E_T = m_9 [h_9 - h_{10} - T_0 (s_9 - s_{10})] \quad (22)$$

$$E_R = m_{13} [h_{13} - h_{12} - T_0 (s_{13} - s_{12})] \quad (23)$$

The exergy balance for the whole ARHP subsystem is:

$$E_{T,in} + W_{P1} + W_{P2} - \sum E_d = E_T + E_R \quad (24)$$

where W_{P2} is the work consumption of the cooling-seawater pump P2,

$$W_{P2} = m_{14}(h_{14} - h_{sw,0}) \approx m_{14}v_{sw,0}(p_{14} - p_0)/\eta_{P2} \quad (25)$$

and $E_{T,in}$ is the thermal exergy input into the ARHP subsystem, which is also the thermal exergy input into the entire ARHP-MEE system,

$$E_{T,in} = m_1[h_1 - h_2 - T_0(T_1 - T_2)] \quad (26)$$

3.2 Mathematical model for the MEE subsystem

3.2.1 Enthalpy, entropy and exergy of saline water

There are mainly two methods to calculate the enthalpy and entropy of saline water. One is based on the empirical correlations equation of specific heat capacity, and the other is based on ideal solution properties.

Expressed as the function of temperature and salinity, the correlation of specific heat capacity at constant pressure is widely used in energy analysis of desalination process (cf. [11, 16]). Care is needed when using this method to ensure that the different working fluids have the same reference standard, as required by chemical thermodynamics [17]. For example, for a typical MEE evaporator (Fig. 5) where feed seawater with temperature T_f , pressure p_f and salinity C_f is separated into two streams: water vapor at T_v and p_v , and brine at T_b , p_b and C_b , by consuming heat energy Q , the enthalpy and entropy changes of the working fluids (excluding the heat source) are

$$\Delta H = m_v h_v + m_b h_b - m_f h_f = L(T_a) + m_v \int_{T_a}^{T_v} c_{p,v}(T) dT + m_b \int_{T_a}^{T_b} c_p(T, C_b) dT - m_f \int_{T_a}^{T_f} c_p(T, C_f) dT \quad (27)$$

$$\Delta S = m_v s_v + m_b s_b - m_f s_f = \frac{L(T_a)}{T_a} + m_v \int_{T_a}^{T_v} c_{p,v}(T) \frac{dT}{T} + m_b \int_{T_a}^{T_b} c_p(T, C_b) \frac{dT}{T} - m_f \int_{T_a}^{T_f} c_p(T, C_f) \frac{dT}{T} \quad (28)$$

where $L(T_a)$ is the latent heat of vaporization at T_a . It is clear that the three terms at the right side of Eqs.(27) and (28) have different reference states: water at T_a , saline water at T_a and C_b , and saline water at

T_a and C_f , respectively. In energy analysis, the reference-state problem for enthalpy can be avoided as done in many publications (cf. [11,16]) by considering that the feed seawater is first heated from T_f to T_b and then partially vaporized at T_b , thus writing the energy balance equation for the typical MEE evaporator as

$$Q = m_f \int_{T_f}^{T_b} c_p(T, C_f) dT + m_v L(T_b) \quad (29)$$

It is more difficult to develop a simple method for calculating the entropy that is needed in the exergy analysis, and we therefore use the second method in this paper. In desalination process, saline water, including rejected brine and feed seawater, has low salinity (lower than 70,000 ppm), and can be dealt with approximately as an ideal solution with acceptable calculation error [18]. The equations are given and validated below.

Fig. 5 Schematic of a typical evaporator in MEE

Based on the properties of ideal solution [19], the specific enthalpy and entropy of saline water at T , p and C can be calculated from

$$h(T, p, C) = \sum_i Y_{s,i} h_{s,i}(T, p) + Y_w h_w(T, p) \quad (30)$$

$$s(T, p, C) = \sum_i Y_{s,i} s_{s,i}(T, p) + Y_w s_w(T, p) - \sum_i R_{s,i} Y_{s,i} \ln Z_{s,i} - R_w Y_w \ln Z_w \quad (31)$$

where Y , Z and R represent mass fraction, molar fraction and gas constant, and the subscripts s and w represent salt and water, respectively. To ensure that different components in the desalination process have the same reference standard, $T^0=298.15\text{K}$ and $p^0=1\text{atm}$ are taken as the reference state, and the enthalpy of formation h_f^0 and absolute entropy s^0 at T^0 and p^0 are introduced,

$$h_s(T, p) = h_{f,s}^0 + [h_s(T, p) - h_s(T^0, p^0)] \quad (32)$$

$$h_w(T, p) = h_{f,w}^0 + [h_w(T, p) - h_w(T^0, p^0)] \quad (33)$$

$$s_s(T, p) = s_s^0 + [s_s(T, p) - s_s(T^0, p^0)] \quad (34)$$

$$s_w(T, p) = s_w^0 + [s_w(T, p) - s_w(T^0, p^0)] \quad (35)$$

The values of h_f^0 and s^0 can be taken from [17].

The ambient seawater state T_0 , p_0 and C_0 is defined as the dead state for exergy analysis. For saline water

at T , p and C , its physical exergy attributed to its temperature and pressure difference from the dead state, and chemical exergy [19] attributed to the concentration difference, can be calculated by

$$e_{ph} = h(T, p, C) - h(T_0, p_0, C) - T_0[s(T, p, C) - s(T_0, p_0, C)] \quad (36)$$

$$e_{ch} = T_0 \left(\sum_i R_{s,i} Y_{s,i} \ln \frac{Z_{s,i}}{Z_{s,i,0}} + R_w Y_w \ln \frac{Z_w}{Z_{w,0}} \right) \quad (37)$$

and the total exergy is:

$$e = e_{ph} + e_{ch} \quad (38)$$

Given in Appendix A is a widely used empirical equation for specific heat capacity of saline water [11]. As mentioned above, the equation is suitable only to calculate the enthalpy/entropy difference between two states with the same salinity. Keeping a constant salinity at 10,000 ppm, 40,000 ppm and 70,000 ppm respectively, the enthalpy and entropy differences between two states with different temperatures were calculated from Eqs. (30)-(35) and Eq. (A1), with the results partially shown in Table 1. Taking the ambient temperature as 20 °C, the exergy difference was also calculated using the two methods and the results also shown in Table 1. Within typical parameters range of MEE ($C \leq 70,000$ ppm, $T = 20-70$ °C), the relative enthalpy/entropy/exergy difference is lower than 2%. It is thus clear that, the saline water can be treated as an ideal solution in thermodynamic modeling of MEE processes, with an acceptable error. This point will be further verified by the good agreement between the simulated performance of the MEE in the present work, and the results from the cited references, with details given in Section 3.4.

Table 1 Enthalpy, entropy and exergy differences calculated from the present model and the empirical equation [Eq. (A1)]

3.2.2 Equations for the MEE subsystem

The working processes in all the effects of MEE are similar, with a general schematic diagram shown in Fig. 6. The mass balance, energy balance and exergy destruction in ED_i are:

$$m_{f,i} + m_{b,i-1} = m'_{v,i} + m_{b,i} \quad (39)$$

$$m_{f,i} C_0 + m_{b,i-1} C_{b,i-1} = m_{b,i} C_{b,i} \quad (40)$$

$$m'_{v,i-1} + m''_{v,i-1} = m_{c,i} \quad (41)$$

$$m'_{v,i-1}h'_{v,i-1} + m''_{v,i-1}h''_{v,i-1} + m_{f,i}h_{f,i} + m_{b,i-1}h_{b,i-1} = m_{c,i}h_{c,i} + m_{b,i}h_{b,i} + m'_{v,i}h_{v,i} \quad (42)$$

$$E_{d,EDi} = T_0(m_{c,i}s_{c,i} + m_{b,i}s_{b,i} + m'_{v,i}s_{v,i} - m_{f,i}s_{f,i} - m'_{v,i-1}s'_{v,i-1} - m''_{v,i-1}s''_{v,i-1} - m_{b,i-1}s_{b,i-1}) \quad (43)$$

The mass balance, energy balance and exergy destruction in F_i are:

$$m_{w,i-1} + m_{c,i} = m_{w,i} + m''_{v,i} \quad (44)$$

$$m_{w,i-1}h_{w,i-1} + m_{c,i}h_{c,i} = m_{w,i}h_{w,i} + m''_{v,i}h''_{v,i} \quad (45)$$

$$E_{d,Fi} = m_{w,i}s_{w,i} + m''_{v,i}s''_{v,i} - m_{w,i-1}s_{w,i-1} - m_{c,i}s_{c,i} \quad (46)$$

The energy balance and exergy destruction in H_i are:

$$(h_{f,i} - h_{f,i+1}) \sum_{j=1}^i m_{f,j} = m'_{v,i}(h_{v,i} - h'_{v,i}) \quad (47)$$

$$E_{d,Hi} = T_0[(s_{f,i} - s_{f,i+1}) \sum_{j=1}^i m_{f,j} + m'_{v,i}(s'_{v,i} - s_{v,i})] \quad (48)$$

Fig.6 Variables of the evaporator, preheater and flashing box of effect i in the MEE subsystem

For the end condenser CD, the energy balance and exergy destruction are:

$$m'_{v,n}h'_{v,n} + m''_{v,n}h''_{v,n} - (m'_{v,n} + m''_{v,n})h_{21} = m_{19}(h_{19} - h_{18}) \quad (49)$$

$$E_{d,CD} = m_{19}(s_{19} - s_{18}) + (m'_{v,n} + m''_{v,n})s_{21} - m'_{v,n}s'_{v,n} - m''_{v,n}s''_{v,n} \quad (50)$$

The pump work consumed and the exergy destruction in pumping processes can be calculated by:

$$W_{Pi} = [m_{in}(h_{P,out} - h_{P,in})]_i \approx [m_{in}v_{in}(p_{P,out} - p_{P,in})/\eta_P]_i \quad (51)$$

$$E_{d,Pi} = [m_{in}(s_{P,out} - s_{P,in})]_i \quad (52)$$

where i refers to pump i ($i=3-6$) in the MEE subsystem (Fig. 2), and the subscripts in and out refer to the working fluid entering and leaving the pump, respectively. The exergy destroyed owing to the physical non-equilibrium between the dead state and the cooling seawater (stream 20), fresh water (streams 22 and 23) and rejected brine (stream 17) is

$$E_{d,emission} = m_{20}e_{20} + m_{22}e_{ph,22} + m_{23}e_{ph,23} + m_{17}e_{ph,17} \quad (53)$$

The maximal work that could be obtained by mixing the produced fresh water and the rejected concentrated seawater in an ideal way, which is also the minimum work consumed in an ideal separation process of the feed seawater, can be calculated from the Gibbs energy difference at ambient states as

shown in [20], or from the sum of the chemical exergies of rejected brine and produced water:

$$W_{\max} = m_{17}e_{ch,17} + (m_{22} + m_{23})e_{ch,22} \quad (54)$$

The two methods have the same result because they have the same mathematical expression after transformation. The exergy balance of the MEE subsystem is

$$E_T + \sum_{i=3}^6 W_{Pi} = \sum E_d + W_{\max} \quad (55)$$

3.3 Performance criteria

The analyzed systems have two useful outputs: fresh water and refrigeration, and performance criteria definition is not straightforward because the products have different physical meaning and units. Obviously, the commonly defined energy efficiency is not suitable here.

Let us examine the suitability of the exergy efficiency for this system. The exergy efficiency, ε , is typically defined as

$$\varepsilon = \frac{W_{\max} + E_R}{E_{T,in} + W_P} \quad (56)$$

Examining the meaning of such an ε , we note the exergy efficiency of a thermal desalination unit is very low, say, about 4% for a common MSF plant run by 99 °C saturated steam [18], while the exergy efficiency of a single-effect absorption refrigeration system is much higher, about 30% in a case study reported in [21]. This means that, about 3.3 kW of driving thermal exergy is needed to produce 1 kW cold exergy by absorption refrigeration, while about 25 kW thermal exergy is needed to produce 1 kW power capacity by thermal desalination. It is thus clear that the exergy efficiency defined in Eq. (56) unreasonably weights water production as a very trivial contribution, and cannot reflect the performance of the water-refrigeration cogeneration systems suitably.

Although these conventional energy and exergy efficiency definitions are thus not applicable to the refrigeration-water combined system, they are applicable to the ARHP subsystem, because it is a refrigeration and heat (all energy quantities, not water) cogenerator. Consequently, if the performance of the MEE unit is specified, it is sufficient, and of general interest, to analyze the performance of ARHP, because it then determines the performance of the entire system. The coefficient of performance and the

exergy efficiency of the refrigeration-heat ARHP subsystem are defined as

$$COP_{RT} = \frac{Q_R + Q_T}{Q_{in} + W_{P,ARHP}} \quad (57)$$

$$\varepsilon_{RT} = \varepsilon_R + \varepsilon_T = \frac{E_R}{E_{T,in} + W_{P,ARHP}} + \frac{E_T}{E_{T,in} + W_{P,ARHP}} \quad (58)$$

where ε_R and ε_T are the exergy efficiency of producing E_R and E_T , respectively.

A dimensionless exergy destruction parameter, ξ , is used to evaluate the process irreversibility:

$$\xi = \frac{E_d}{E_{T,in} + W_P} \quad (59)$$

We also use the Refrigeration-Water Ratio (RWR), defined as

$$RWR = \frac{Q_R}{m_w} \text{ [kJ/kg]} \quad (60)$$

3.4 Model validation

The simulation was carried out using the Engineering Equation Solver (EES) software [22]. The properties of water/steam and the properties, except enthalpy and entropy, of LiBr-H₂O solution were taken from the correlations provided by EES. The enthalpy and entropy of LiBr-H₂O solution were taken from Kaita [23]. The boiling elevation of brine and the non-equilibrium allowance of flash evaporation in the flashing box were taken from [11].

The computerized models were first validated by checking the relative errors of mass, energy and exergy balance of each component and the entire system,

$$r_m = \left| \frac{\sum m_{in} - \sum m_{out}}{\sum m_{in}} \right| \quad (61)$$

$$r_{En} = \left| \frac{\sum E_{n,in} - \sum E_{n,out}}{\sum E_{n,in}} \right| \quad (62)$$

$$r_E = \left| \frac{\sum E_{in} - \sum E_{out} - \sum E_d}{\sum E_{in}} \right| \quad (63)$$

where they were found to be $< 10^{-5}$.

Since the ARHP-MEE combined system is new, no theoretical or experimental data can be found for model validation. A somewhat similar case was available in [5], with insufficient information to run our model. It is seen from Fig. 2, however, that the two subsystems, ARHP and MEE, are relatively independent, and thus can be validated separately. Comparison between the configurations of the ARHP subsystem (Fig. 2) and the AR system (Fig. 3) shows that, although operating within different temperature ranges, ARHP and AR have the same working process and thus the same mass and energy balances equations, making it feasible to validate the present model of the ARHP through the available performance results of a typical AR that can be found in many publications [24, 25]. Two cases are shown in Table 2. Exhibiting relative differences within $\pm 2\%$, the results indicate good agreement between the model predictions and the available data [24, 25]. As to the AHP subsystem in AHP-MEE, the main components are generator, absorber and solution heat exchanger, working in the same way as that in AR and ARHP. The results in Table 2 validated the model of the generator, absorber and solution heat exchanger, thus also validated the modeling of the AHP in our present study.

Table 2 Comparison of model predictions with data from references for AR (ARHP) system

To validate the present model for MEE, the model predictions for four cases are compared with the available data from [16], [26] and [27], with the results shown in Table 3. In [16] and [26] the system was, however, MEE coupled with a steam jet ejector, not stand-alone MEE unit. After referring to the operation parameters of the steam jet ejector and the whole system, we calculated the mass flow rate of the heating steam, heat energy input to MEE and performance ratio of MEE, thus obtaining enough information for model validation. It can be seen from Table 2 that the model predictions compare well with the data in the literature.

Table 3 Comparison of model predictions with data from references for MEE unit

4. Conclusions

Motivated by the good synergetic potential of energy/exergy utilization through the combination of the LiBr-H₂O refrigeration unit, LiBr-H₂O heat pump, and low-temperature MEE, we proposed here a combined refrigeration and water system, ARHP-MEE, driven by low-grade heat. After illustrating the integration logic, the system configuration is introduced, and the mathematical model is presented based

on the principles of mass conservation, first and second laws of thermodynamics. The model predictions are in good agreement with the available published data.. The model is used to study the performance of the combined system in Part 2 of the article.

Acknowledgement

The authors gratefully acknowledge the support of the National Natural Science Foundation of China (Project No. 50676023), the Science and Technology Innovation Platform Foundation of Fujian Province, China (Project No. 2009H2006) and the Specialized Foundation for Creative Team of Young and Middle-aged Teachers of Jimei University, China (Project No. 2009A002).

Appendix A. Empirical equation for constant pressure specific heat capacity of saline water [11]

$$c_p = (a + bT + cT^2 + dT^3)/1000 \quad (A1)$$

The variables a , b , c and d are expressed as a function of salinity of saline water:

$$a = 4206.8 - 6.6197C + 1.2288 \times 10^{-2} C^2$$

$$b = -1.1262 + 5.4178 \times 10^{-2} C - 2.2719 \times 10^{-4} C^2$$

$$c = 1.2026 \times 10^{-2} - 5.3566 \times 10^{-4} C + 1.8906 \times 10^{-6} C^2$$

$$d = 6.8777 \times 10^{-7} + 1.517 \times 10^{-6} C - 4.4268 \times 10^{-9} C^2$$

where c_p is in kJ/kg °C, T in °C and C in g/kg. The equation is valid over salinity range of 20-160 g/kg and temperature range of 20-180°C.

References

- [1] Horlock JH. Cogeneration—Combined Heat and Power (CHP): Thermodynamics and Economics. New York: Pergamon; 1987
- [2] Husain A. Integrated Power and Desalination Plants, The Encyclopedia of Life Support Systems (EOLSS). UK: Oxford; 2003
- [3] Wu DW, Wang RZ. Combined cooling, heating and power: A review. Progress in Energy and Combustion Science 2006; 32: 459–95
- [4] Aly SE. A study of a new thermal vapor compression/multi-effect stack (TVC/MES) low temperature

- distillation system. *Desalination* 1995; 103: 257-63
- [5] Gude VG, Nirmalakhandan N. Combined desalination and solar-assisted air-conditioning system. *Energy Conversion and management* 2008; 49: 3326-30
- [6] Hou S, Li H and Zhang H. An open air-vapor compression refrigeration system for air-conditioning and desalination on ship. *Desalination* 2008; 222: 646-55
- [7] Shen C, Li X, Wang H, et al. Study on the seawater desalination system combined with LiBr absorption-type refrigerator. *Petro-chemical Equipment* 2005; 34: 39-41 (In Chinese)
- [8] Hu S, Yin Z, Wang G. Combined operating of heat pump air conditioning and seawater desalination system. *Journal of Heating, Ventilating and Air Conditioning* 2006; 36: 30-33 (In Chinese)
- [9] Dai Y. *Technology and Application of Lithium Bromide Absorption Refrigeration*. Beijing: Mechanical Industry; 2002 (in Chinese)
- [10] Kronenberg G, Kokiec F. Low-temperature distillation processes in single- and dual-purpose plants. *Desalination* 2001, 136: 189-97
- [11] El-Dessouky H, Ettouney H. *Fundamentals of Salt Water Desalination*. Amsterdam: Elsevier; 2002
- [12] Alarcon-Padilla D, Garcia-Rodriguez L, Blanco-Galvez J. Assessment of an absorption heat pump coupled to a multi-effect distillation unit within AQUASOL project. *Desalination* 2007; 212: 303-10
- [13] Mandani F, Ettouney H, El-Dessouky H. LiBr-H₂O absorption heat pump for single-effect evaporation desalination process. *Desalination* 2000; 128: 161-76
- [14] Su J, Han W, Jin H. A new seawater desalination system combined with double-effect absorption heat pump. *Journal of Engineering Thermophysics* 2008; 29: 377-80 (In Chinese)
- [15] Cengel YA, Boles MA. *Thermodynamics - An Engineering Approach* (4th Edition). New York: McGraw Hill; 2002
- [16] Alasfour FN, Darwish MA, Bin Amer AO. Thermal analysis of ME-TVC+MEE desalination systems. *Desalination* 2005; 174: 39-61
- [17] Chang R. *Chemistry* (5th Edition). New York: McGraw Hill; 1994
- [18] Kahraman N, Cengel YA. Exergy analysis of a MSF distillation plant. *Energy Conversion and Management* 2005; 46: 2625–36
- [19] Zhu M. *Exergy analysis of energy systems*. Beijing: Qinghua University; 1988 (In Chinese)
- [20] Wang Y, Lior N. Performance analysis of combined humidified gas turbine power generation and multi-effect thermal vapor compression desalination systems — Part 1: The desalination unit and its

combination with a steam-injected gas turbine power system. *Desalination* 2006; 84-104

[21] Kilic M, Kaynakli O. Second law-based thermodynamic analysis of water-lithium absorption refrigeration system. *Energy* 2007; 32: 1505-12

[22] F-chart Software, <http://www.fchart.com/ees/ees.shtml/> (accessed on Jan. 18, 2010)

[23] Kaita Y. Thermodynamic properties of lithium bromide-water solution at high temperatures. *International Journal of Refrigeration* 2001; 24: 374-90

[24] Florides GA, Kalogirou SA, Wrobel LC. Design and construction of a LiBr water absorption machine. *Energy Conversion and Management* 2003; 44: 2483-508

[25] Yan Q, Shi W, Tian C. Refrigeration technology in air conditioning (3rd Edition). Beijing: China Architecture Industry; 2004 (In Chinese)

[26] Darwish MA, El-Dessouky H. The heat recovery thermal vapour-compression desalination system: a comparison with other processes. *Applied Thermal Engineering*, 1996; 16: 523-37

[27] Wang C. Performance analysis of low-temperature multi-effect evaporation seawater desalination plants. Master's Thesis. Beijing: North China Electric Power University; 2006 (In Chinese)

Figure captions

Fig. 1 Schematics of AR, AHP and ARHP

Fig. 2 Schematic diagram of the ARHP-MEE cogeneration system

Fig. 3 Schematic diagram of the AR refrigeration-only system

Fig. 4 Schematic diagram of the AHP-MEE water-only system

Fig. 5 Schematic of a typical evaporator in MEE

Fig. 6 Variables of the evaporator, preheater and flashing box of effect i in MEE subsystem

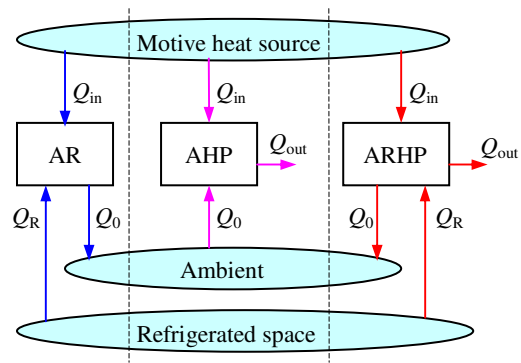


Fig. 1 Schematics of AR, AHP and ARHP

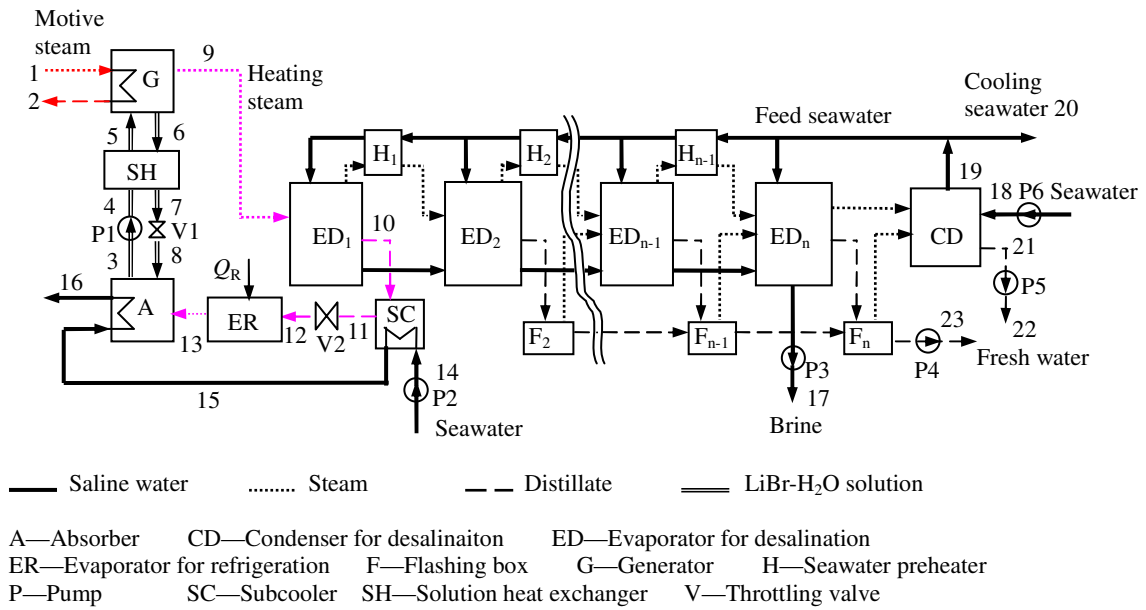
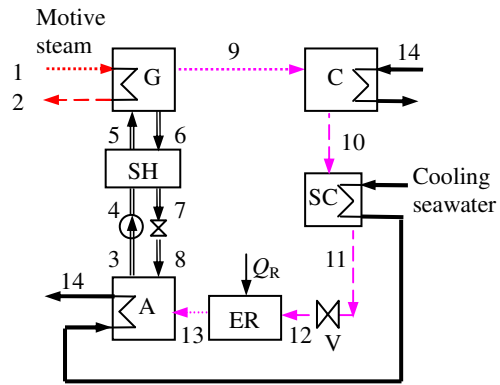
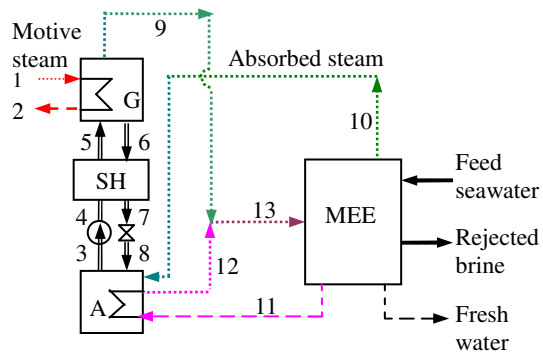


Fig. 2 Schematic diagram of the ARHP-MEE cogeneration system



*C represents condenser, with the other notes the same as Fig. 2.

Fig. 3 Schematic diagram of the AR refrigeration-only system



* The notes are the same with Fig. 2.

Fig. 4 Schematic diagram of the AHP-MEE water-only system

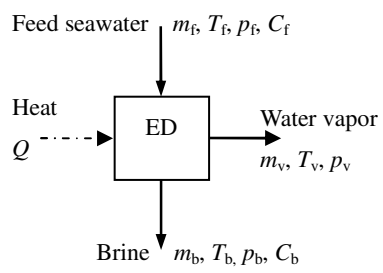


Fig. 5 Schematic of a typical evaporator in MEE

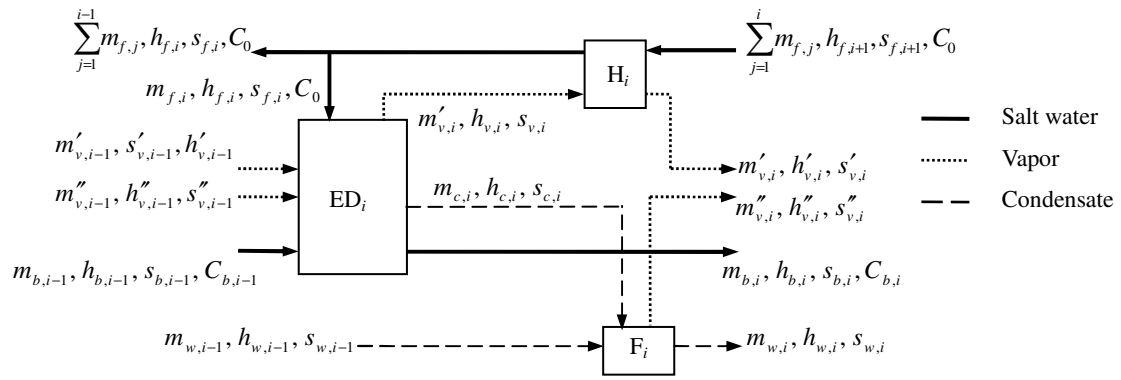


Fig.6 Variables of the evaporator, preheater and flash box of effect i in MEE subsystem

Table captions

Table 1 Enthalpy, entropy and exergy differences calculated from the present model and the empirical equation [Eq. (A1)]

Table 2 Comparison of model predictions with data from references for AR (ARHP) system

Table 3 Comparison of model predictions with data from references for MEE unit

Table 1 Enthalpy, entropy and exergy differences calculated from the present model and the empirical equation [Eq.(A1)]

($T_a=20$ °C, $p_a=p_b=1$ atm)

T_b (°C)	Δh_{ab} (kJ/kg)		Difference (%)	Δs_{ab} (kJ/kg K)		Difference (%)	Δe_{ab} (kJ/kg)		Difference (%)
	Model	Eq. (A1)		Model	Eq. (A1)		Model	Eq. (A1)	
C=10,000 ppm									
30	41.41	41.31	0.24	0.1389	0.1386	0.24	0.691	0.689	0.26
40	82.82	82.61	0.26	0.2733	0.2726	0.26	2.703	2.695	0.29
50	124.22	123.91	0.25	0.4034	0.4024	0.25	5.953	5.937	0.27
60	165.62	165.23	0.24	0.5296	0.5284	0.24	10.37	10.34	0.25
70	207.05	206.58	0.22	0.6521	0.6507	0.22	15.88	15.84	0.22
C=40,000 ppm									
30	40.16	39.76	1.01	0.1347	0.1333	1.01	0.670	0.663	1.00
40	80.31	79.55	0.95	0.2650	0.2625	0.95	2.621	2.597	0.93
50	120.46	119.40	0.89	0.3912	0.3878	0.89	5.773	5.724	0.84
60	160.60	159.28	0.83	0.5136	0.5093	0.83	10.05	9.975	0.77
70	200.77	199.22	0.78	0.6324	0.6274	0.79	15.40	15.29	0.71
C=70,000 ppm									
30	38.90	38.34	1.48	0.1305	0.1286	1.48	0.649	0.640	1.45
40	77.80	76.75	1.37	0.2567	0.2533	1.37	2.539	2.506	1.31
50	116.69	115.24	1.26	0.3790	0.3742	1.27	5.592	5.527	1.17
60	155.59	153.78	1.18	0.4975	0.4917	1.18	9.738	9.635	1.06
70	194.50	192.37	1.11	0.6126	0.6059	1.12	14.91	14.77	0.99

Table 2 Comparison of model predictions with data from references for AR (ARHP) system

Main parameters input	Case 1 [24]			Case 2 [25]		
Cold capacity (kW)	10			1000		
Evaporation temperature (°C)	6			5		
Condensation temperature (°C)	44.3			46		
Solution temperature at generator outlet (°C)	90			102.2		
Solution concentration difference ΔX (%)	5			4.5		
Cold-side temperature difference of SH (°C)	19.9			25		
Main parameters output	[24]	Model	Difference (%)	[25]	Model	Difference (%)
Concentration of strong solution (%)	60	60.4	--	64	64.6	--
Mass flow of weak solution (kg/s)	0.053	0.052	-1.9	6.127	6.196	1.1
Mass flow of strong solution (kg/s)	0.0486	0.0477	-1.9	5.696	5.764	1.2
Heat load of generator (kW)	14.2	13.97	-1.6	1505	1530	1.7
Heat load of absorber (kW)	13.42	13.34	-0.6	1431	1456	1.7
Heat load of solution heat exchanger (kW)	3.30	3.24	-1.8	348.2	351.9	1.1
Heat load of condenser (kW)	10.78	10.63	-1.4	1074	1074	0
Work consumption of solution pump (kW)	0.0003	0.0004	--	--	0.03	--
Work consumption of cooling-water pump (kW)	--	0.021	--	--	2.30	--
Coefficient of performance	0.704	0.715	1.6	0.665	0.653	-1.8

The adiabatic efficiency of the pump was taken as 100% in [24], and 75% in present model predictions.

Table 3 Comparison of model predictions with data from references for MEE unit

Calculation conditions	Case 1 [16]	Case 2 [16]	Case 3 [26]	Case 4 [27]
Effect number	6	6	4	9
Top brine temperature (°C)	61.8	61.8	58.8	65
Evaporation temperature of last effect (°C)	42.8	42.8	46.8	39
Salinity of feed seawater (ppm)	47800*	47800*	47800*	36000
Salinity of rejected brine (ppm)	71500*	71500*	71500*	54000
Thermal energy input to MEE (kW)	5745.7	5745.7	4511.2	2338
Mass flow of heating steam (kg/s)	2.36	2.36	1.86	1
Calculation results				
PR from references	5.79	5.11	3.54	6.15
PR from present model	5.61	5.05	3.61	6.34
Difference (%)	-3.1	-1.2	2.0	3.1

* Assumed values based on the context of the references.